Resonances in pulsatile channel flow with an elastic wall

Duo Xu,[1, 2, *] Thomas Seeböck,[2] and Marc Avila[1, 2, †]

[1] *University of Bremen, Center of Applied Space Technology and Microgravity (ZARM), 28359 Bremen, Germany*
[2] *Friedrich-Alexander-Universität Erlangen-Nürnberg, 91058 Erlangen, Germany*

(Dated: June 20, 2019)

The interaction between fluid and elastic solids is ubiquitous in aerospace, mechanical and civil engineering. Pulsations in fluid velocity may interact with the natural frequency of the solids and lead to catastrophic events, such as the crumbling of the Tacoma-Narrows bridge. In nature, fluid-structure interaction is exploited by microorganisms to swim and it enables a reduction of the pressure and flow-rate pulsations of blood as this is transported from the heart to the periphery of the body. Here we simplify this complex problem and consider the dynamics of a membrane clamped between two rigid segments in a channel. Fluid flow driven by a pulsatile pressure difference and after initial transients determined by the viscosity of the fluid, the membrane pulsates synchronously with the driving frequency. The amplitude of the oscillation varies non-monotonously with the governing parameters and exhibits strong resonances. At the resonance point, the flow rate over a cycle is larger than for steady flow in a rigid channel with the same pressure loss. We show that the oscillation motions of the elastic membrane can be accurately modeled with the equation of a forced damped harmonic oscillator. All key features of the system are predicted by the model: oscillation amplitude, phase between pressure driving and response of the membrane, resonance point and vanishing of the resonance as the viscous drag becomes dominant.

Fluid flows through elastic conduits are of engineering and physiological relevance. Locally in the arterial tree, fluid-structure-interaction (FSI) can be harmful and has been associated with the rupture of aneurysms [1] and atherosclerotic plaque rupture in arterial stenoses, which can cause heart attack or stroke [2]. On the other hand, in collapsed blood vessels FSI is exploited to regulate the blood supply to internal organs [3], and to help returning blood to the heart during diastole [4]. The fundamental setup to investigate the nonlinearly coupled dynamics of the fluid and the vessels is the Starling resistor [5], which consists of an elastic tube mounted between two rigid tubes in a pressure chamber. In the Starling resistor the fluid is driven at a steady flow rate, but if the flow rate exceeds a critical value, self-excited oscillations arise spontaneously [6–8]. A widely used system exhibiting similar dynamics is collapsible channel flow, where fluid is driven between a rigid bottom wall and an upper wall composed of a flexible externally pressurized membrane clamped between two rigid sections [9, 10]. To the best of our knowledge, the fully coupled nonlinear interaction between pulsatile flow and an elastic wall has neither been investigated in channels nor in tubes.

In this *Letter*, we perform numerical simulations of a collapsible channel with a pulsatile pressure difference and consider the effect of all relevant governing parameters. We show that the membrane oscillation exhibits strong resonances, reminiscent of a forced damped harmonic oscillator. Guided by this analogy, we present a simple mathematical model which successfully predicts the oscillation amplitude of the membrane, the phase lag between the amplitude and the imposed pressure and also the vanishing of resonance as the damping is increased.

A fluid of kinematic viscosity ν and density ρ is driven by a pulsatile pressure difference of average $\Delta P_0 = \langle P_{\rm in} - P_{\rm out} \rangle$ and frequency ω through a two-dimensional channel of length l and height h (see Fig. 1b). The lower channel wall is rigid, whereas a membrane of length $l_{\rm m}/h = 10$ is clamped between two rigid segments at the upper wall and is pressurized with an external pressure $P_{\rm ext}$ from outside. The fluid motion is governed by the incompressible Navier–Stokes equations, which in dimensionless form read

$$\frac{\partial u_j}{\partial t} + u_i \frac{\partial u_j}{\partial x_i} = -\frac{\partial p}{\partial x_j} + \frac{\partial^2 u_j}{\partial x_i^2}, \quad \frac{\partial u_j}{\partial x_j} = 0. \qquad (1)$$

Here x_1 (x_2) is the horizontal (vertical) coordinate and summation over i is assumed. Lengths were scaled by the channel height h, whereas viscous scales were used for time h^2/ν and pressure $\rho\nu^2/h^2$. The dimensionless driving pressure difference between inlet and outlet reads

$$\Delta P(t) = Re \frac{12\, l}{h} \left(1 + \sin\left(Wo^2\, t\right)\right), \qquad (2)$$

where $Wo = h\sqrt{\omega/\nu}$ is the Womersley number and $Re = h\bar{u}/\nu$ is the Reynolds number based on the mean velocity of laminar Poiseuille flow $\bar{u}$ driven by the steady pressure gradient $\Delta P_0/l$ in the undeformed channel. The boundary conditions for the velocity are no-slip at the walls, whereas parallel flow is assumed at the upstream and downstream boundaries. The length of the two rigid segments clamping the membrane was chosen long enough not to influence the emerging flow patterns.

We consider a thin massless membrane of Young modulus E and Poisson ratio β, which deforms because of the constant external pressure $p_{\rm ext}$ acting on its upper side and of unsteady viscous and pressure forces exerted by the fluid on its lower side. The resulting load vector is made dimensionless with the effective elastic modulus

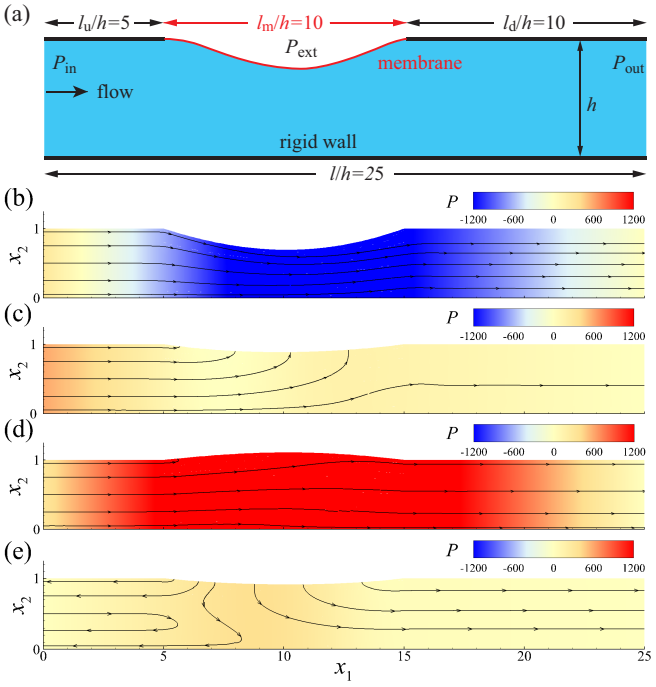

FIG. 1. (Color online) (a) Sketch of fluid flow in a collapsible channel with an externally pressurized membrane clamped between two rigid walls. The flow is driven by a pulsatile pressure difference. Contour of pressure after the initial transients for $t/T = 0$ (b), 0.25 (c), 0.5 (d) and 0.75 (e), and streamlines are marked in solid lines with arrows.

$$E_{\text{eff}} = E/(1-\beta^2),$$

$$f_j = -P_{\text{ext}} \cdot n_j + \frac{1}{H}\left[P \cdot n_j - \left(\frac{\partial u_i}{\partial x_j} + \frac{\partial u_j}{\partial x_i}\right) n_i\right]. \quad (3)$$

Here n_j is the normal vector to a point on the membrane, $P_{\text{ext}} = p_{\text{ext}}/E_{\text{eff}}$ is the dimensionless external pressure, and $H = h^2 E_{\text{eff}}/(\rho\nu^2)$ is the ratio of the effective modulus to the viscous pressure scale and is thus a material parameter. In studies of flows in collapsible channels, it is customary to use the parameter $Q = Re/H$, which is the ratio between viscous and elastic forces.

The membrane is subject to dimensionless axial prestress $\sigma_0 = 10^3$ to assume incrementally linear behavior and its deformation is guided by the principle of virtual displacement. A dimensionless Lagrangian coordinate ξ is used to parametrize the membrane. At time t, the Eulerian coordinate of a point ξ in the membrane is given by $R_i(\xi,t) = r_i(\xi) + d_i(\xi,t)$, where $r_i(\xi)$ denotes the position vector $[\xi,1]^T$ for the undeformed membrane and $d_i(\xi,t)$ is the displacement vector [9]. The motion for the membrane is governed by the following dimensionless equation

$$\int_0^{\frac{l_m}{h}} \left((\sigma_0+\gamma)\delta\gamma + \frac{1}{12}\epsilon^2\kappa\,\delta\kappa - \frac{1}{\epsilon} f_j \cdot \delta R_j \Lambda\right) d\xi = 0, \quad (4)$$

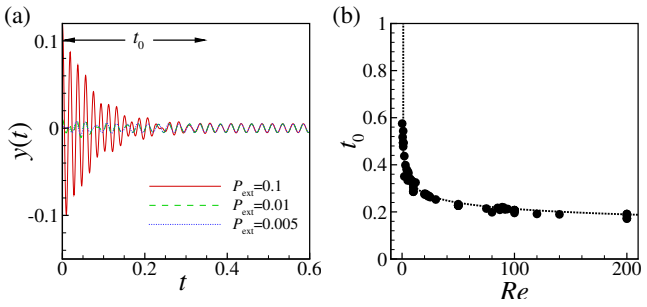

FIG. 2. (Color online) (a) Time series of vertical displacement of the membrane at $Re = 50$, $Wo = 15.81$, $Q = 10^{-5}$, and three different external pressures ($P_{\text{ext}} = 0.1$, 0.01 and 0.005) as a function of time. The time-averaged displacements after transients (0.877, 0.990 and 0.996) are subtracted. (b) Decay time of initial transients t_0 at $P_{\text{ext}} = 0.1$ and $Q = 10^{-5}$ as function of Reynolds number for $Wo \in [0.32, 63.25]$. The dashed line shows the curve $0.423\,Re^{-1/6}$.

where $\epsilon = 0.01$ is the dimensionless thickness of the membrane, $\gamma = \partial d_1/\partial\xi + 0.5[(\partial d_1/\partial\xi)^2 + (\partial d_2/\partial\xi)^2]$ the strain tensor, and $\kappa = [(\partial^2 d_2/\partial\xi^2)(1+\partial d_1/\partial\xi) - (\partial^2 d_2/\partial\xi^2)(\partial d_2/\partial\xi)]/\Lambda$ the bending tensor, with $\Lambda = [(1+\partial d_1/\partial\xi)^2 + (\partial d_2/\partial\xi)^2]^{1/2}$. We solve the time-dependent fully coupled fluid-structure problem with the open-source library *oomph-lib* [11, 12], which allows us to study large displacements of the membrane.

We investigated the dynamics of the system by monitoring the vertical displacement of the membrane at its midpoint as a proxy of the deformation. Initially, the membrane is undeformed and the velocity field is parabolic laminar Poiseuille flow. Subsequently, the external pressure pushes the membrane inward and this undergoes damped oscillations before settling into a time-periodic (harmonic) motion. Fig. 2(a) shows that the final amplitude of the membrane oscillations $y(t)$ is independent of the external pressure, so from now we set $P_{\text{ext}} = 0.1$. Note that this behavior is in contrast to self-excited oscillations generated by a constant pressure gradient [13]. The duration of the initial transients t_0 is on the order of a viscous time unit, suggesting that the adjustment toward a harmonic oscillation is predominantly controlled by the viscosity of fluid. Overall, t_0 is largely unaffected by the pulsation frequency and diminishes slowly as Re increases (see Fig. 2b).

We now focus on the dynamics of the steady-state oscillations after transients. The symbols in Fig. 3(a) shows the amplitude of the oscillations G against Wo for five different Reynolds numbers and $Q = 10^{-5}$. As the driving frequency increases, the oscillation amplitude of the membrane first increases and then decreases. Note also that there is a phase shift ϕ between $\Delta P(t)$ and $y(t)$, which depends on Wo. In all cases, when the amplitude of the response features a sharp peak, the pressure difference and membrane displacement are exactly out of phase ($\phi = \pi/2$).

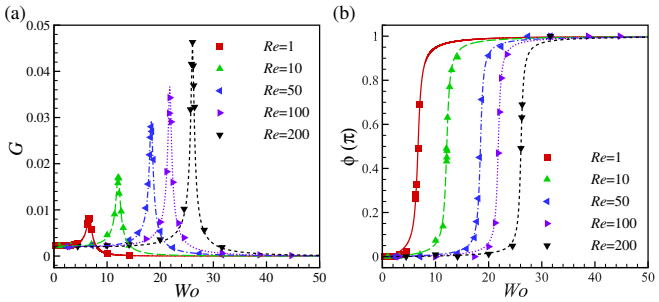

FIG. 3. (Color online) (a) Amplitude of the steady-state oscillations as a function of Wo for several Re as indicated in the legend. Here $P_{\rm ext} = 0.1$ and $Q = 10^{-5}$. (b) Phase shift ϕ as a function Wo. Symbols denote the simulation data and lines are from the harmonic oscillator model, with eq. (9) for G and (10) for ϕ, respectively.

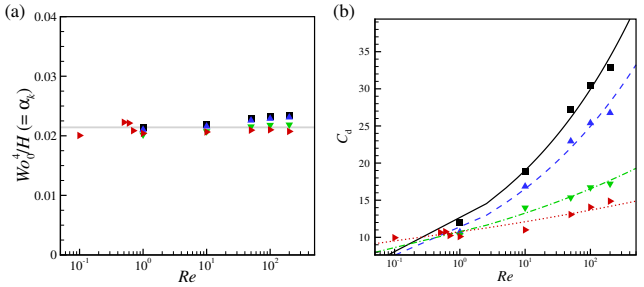

FIG. 4. (Color online) (a) Dimensionless eigenfrequency Wo_0 of the collapsible channel against Re for $Q = 10^{-5}$ (black squares and black circles), $Q = 2 \times 10^{-5}$ (blue up-triangles), $Q = 10^{-4}$ (green down-triangles) and $Q = 2\times10^{-4}$ (red right-triangles). The gray solid-line shows $\alpha_k = 0.02$. (b) The drag coefficients $C_{\rm d}$ varying with Re where the symbols, the same as Fig. 5, lines are from power law fitting.

The response of the membrane deformation is reminiscent of the response of the forced damped harmonic oscillator in classical mechanics [14], which consists of a mass $\widetilde{m}$ attached to a spring with stiffness coefficient $\widetilde{k}$ subject to an external harmonic force of amplitude $\widetilde{f}$ and frequency ω. In addition, the motion of the mass is damped by viscous force with damping coefficient c. The governing equation of the harmonic oscillator is

$$\widetilde{m}\frac{\partial^2\widetilde{y}}{\partial\widetilde{t}^2} = -c\frac{\partial\widetilde{y}}{\partial\widetilde{t}} - \widetilde{k}\,\widetilde{y} + \widetilde{f}\sin\omega\widetilde{t}, \tag{5}$$

where $\widetilde{y}$ is the instantaneous displacement of the mass with respect to the equilibrium position. In what follows, we explore an analogy between the collapsible channel driven by a pulsatile pressure difference and the driven harmonic oscillator. In this analogy, the displacement of the membrane's midpoint $y(t)$ is assumed to exhibit dynamics similar to the spring displacement $\widetilde{y}(t)$ in the harmonic oscillator.

In our model, the spring constant k is assumed proportional to the effective Young modulus of the membrane and to its length, i.e. $\tilde{k} = A_{\rm k}\,E_{\rm eff}\,l_{\rm m}$, whereas the mass is assumed proportional to the mass of fluid beneath the membrane $\tilde{m} = A_{\rm m}\,\rho\,l_{\rm m}\,h^2$. The main driving force is expected to be proportional to the pressure force acting on the membrane $\tilde{f} = A_{\rm f}\,\rho\nu\,\bar{u}\,l_{\rm m}$. Note that because the flow is laminar, we choose the viscous scale $\rho\nu\,\bar{u}/h$ for the pressure. The scaling of the viscous damping coefficient c is unclear a priori, so this is left as unknown for the time being.

Plugging in the expressions for $\tilde{m}$, $\tilde{f}$ and $\tilde{k}$ above into (5) and rendering the equation dimensionless by rescaling lengths with h, velocities with $\bar{u}$ and time with h^2/ν, we obtain the following model

$$\frac{\partial^2 y}{\partial t^2} + C_{\rm d}\frac{\partial y}{\partial t} + \left(Wo_0^4\right) y = \alpha_f Re\,\sin\left(Wo^2\,t\right), \tag{6}$$

with $\alpha_f = A_{\rm f}/A_{\rm m}$ and the drag coefficient $C_{\rm d} = c/(A_{\rm m}\,\rho\nu\,l_{\rm m})$. The model predicts that the eigenfrequency Wo_0 of the collapsible channel depends on the material properties of the fluid-structure interaction as

$$Wo_0 = (\alpha_k H)^{1/4}, \tag{7}$$

with the constant $\alpha_k = A_{\rm k}/A_{\rm m}$. The accuracy of the assumptions in our model can be assessed by fitting the simulation data with the well-known analytic steady-state solution of (6)

$$y(t) = G\cdot\sin\left(Wo^2\cdot t - \phi\right), \tag{8}$$

where

$$G = \frac{\alpha_f Re}{\sqrt{\left(Wo_0^4 - Wo^4\right)^2 + C_{\rm d}^2\,Wo^4}}, \tag{9}$$

is the amplitude of the oscillations (typically referred to as gain) and

$$\phi = \tan^{-1}\left[\frac{C_{\rm d}\,Wo^2}{Wo_0^4 - Wo^4}\right] \tag{10}$$

is the phase delay between driving force and response. In summary, there are three fit parameters, of which two (α_k and α_f) should be constant according to the model, whereas the drag coefficient $C_{\rm d}$ is expected to depend on the flow parameters and particularly on the Reynolds number.

The lines in Fig. 3a show the best fits of the gain (9) to the oscillation amplitude obtained from the numerical simulations. Indeed, we find that $\alpha_f \approx 4.2$ and $\alpha_k \approx 0.02$ are constants adjusting all data sets, whereas $C_{\rm d}$ depends on Re. The fitted values of α_f, α_k and $C_{\rm d}$ also render excellent approximations of the phase delay (see lines in Fig. 3b). Together these results suggest that the dynamics of the pulsatile collapsible channel can be accurately modeled with a harmonic oscillator. Despite the wide ranges of Wo and Re covered in Fig. 3, all these

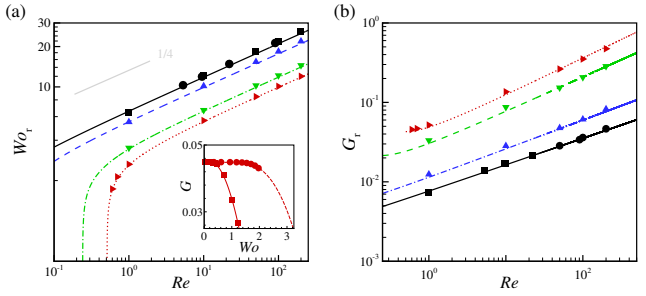

FIG. 5. (Color online) (a) Resonant points for $Q = 10^{-5}$ (black squares and black circles), $Q = 2 \times 10^{-5}$ (blue up-triangles), $Q = 10^{-4}$ (green down-triangles) and $Q = 2\times10^{-4}$ (red right-triangles). The lines correspond to Eq. 9 and 11 with $\alpha_f = 4.2$ and $\alpha_k = 0.02$. (a) (Re, Wo_r), where the inset shows that for $Q = 2 \times 10^{-4}$ at $Re = 0.1$ (squares) and 0.5 (circles) G increases and saturates at a constant as Wo decreases. (b) The oscillation amplitudes G_r against the Reynolds number Re at the resonance.

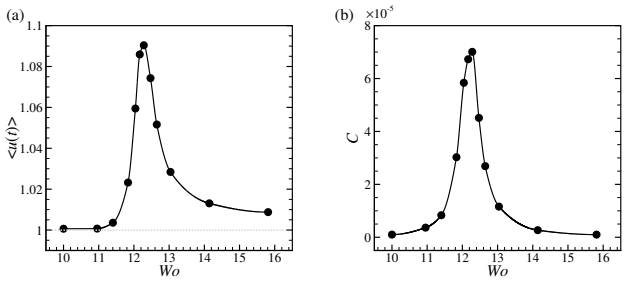

FIG. 6. (Color online) (a) Averaged streamwise fluid velocity $\langle u(t) \rangle$ against Womersley number Wo for $Re = 100$, $Q = 10^{-4}$ $(H = 10^6)$ and $P_{\text{ext}} = 0.012$. (b) Flow compliance.

simulations were obtained for $Q = 10^{-5}$. This raises the question of whether the model captures the dependency on Q as well, which was investigated here by performing additional sets of simulations for $Q = 2 \times 10^{-5}$, 10^{-4} and 2×10^{-4}. Of particular interest is the eigenfrequency prediction (see 7 and recall that $H = Re/Q$). Figure fig:Wo0a confirms our prediction and shows that the eigenfrequency of the collapsible channel depends only on material parameters at low Reynolds numbers $Re \leq 10$, whereas at higher Re small but noticeable differences among the data sets for different Q are observed. On the other hand, the data reveal a complex dependence of the friction coefficient on Re and Q. In particular, C_{d} follows a power-law of the Reynolds number, in which both pre-factor and exponent depend on Q (see Fig. 4b).

A well-known feature of the driven harmonic oscillator is that resonances disappear as the damping increases. More specifically, the resonant Womersley number

$$Wo_{\text{r}} = (\, Wo_0^4 - C_{\text{d}}^2/2)^{1/4}, \tag{11}$$

maximizing the gain G (in Eq. 9) disappears when $C_{\text{d}} \geqslant \sqrt{2}\, Wo_0^2$. This process of extinction of resonances occurs also in the collapsible channel. Figure 5a shows that as C_{d} increases, the resonance peak becomes wider until it disappears. When this happens the maximum gain is oobtained in the quasi-static limit $Wo \to 0$ (see inset of Fig. 5a). When $C_{\text{d}} \ll \sqrt{2}\, Wo_0^2$, the resonant frequency is close to the eigenfrequency ($Wo_{\text{r}} \approx Wo_0$), and in view of Eq. 7, $Wo_{\text{r}} \propto Re^{1/4}$, as exhibited by our data (see the gray line in Fig. 5a). In this scaling regime, the maximum (resonant) gain $G_r \propto C_{\text{d}}^{-2}$ becomes a Q-dependent power-law of the Reynolds number, with exponent 0.33 to 0.42 as Q increases from 10^{-5} to 2×10^{-4}.

The relationship between the driving pressure difference and the flow rate is important for fluid transport and has attracted much attention in studies of blood flows, where it is usually described with windkessel models [15]. Figure 6a shows the time-averaged streamwise velocity as a function of the Wommersly number. Here all other parameters were kept fixed, so that this figure illlustrates the effect of changing the pulsation frequency in a physical experiment. The external pressure was chosen such that the membrane oscillated with zero average deformation (i.e. about the height of the solid wall segments). Interestingly, the mean velocity is higher than that of a rigid channel driven with a constant pressure difference, resulting in an enhancement of nearly 10% close to the resonance point. Similarly, the compliance C, obtained by the volume change of the channel over the corresponding pressure change (through a least-squared linear-fitting), features also a strong dependence on the frequency (see Fig. 6b), a feature clearly not present in windkessel models.

In summary, we have shown that the dynamics of pulsatile flow in a channel with an elastic wall, which is a canonical model for blood flow in elastic vessels, exhibits complex dependencies on the material and flow parameters. Despite this complexity, the dynamics of the membrane can be entirely described with a simple harmonic oscillator model.

D.X. gratefully acknowledges the support from Alexander von Humboldt Foundation (3.5-CHN/1154663STP).

* duo.xu@zarm.uni-bremen.de
† marc.avila@zarm.uni-bremen.de

[1] H.-C. Han, J. K. W. Chesnutt, J. R. Garcia, Q. Liu, and Q. Wen, Annals of Biomedical Engineering **41**, 1399 (2013).
[2] D. N. Ku, Annual Review of Fluid Mechanics **29**, 399 (1997).
[3] A. H. Shapiro, Journal of Biomechanical Engineering **99**, 126 (1977).
[4] D. P. Casey and E. C. Hart, The Journal of Physiology **586**, 5045 (2008).
[5] F. P. Knowlton and E. H. Starling, The Journal of Physiology **44**, 206 (1912).

[6] C. D. Bertram, Respiratory Physiology & Neurobiology **163**, 256 (2008).
[7] M. Heil and J. Boyle, Journal of Fluid Mechanics **652**, 405 (2010).
[8] P. S. Stewart, S. L. Waters, and O. E. Jensen, European Journal of Mechanics-B/Fluids **28**, 541 (2009).
[9] O. E. Jensen and M. Heil, Journal of Fluid Mechanics **481**, 235 (2003).
[10] M. Heil and A. L. Hazel, Annual Review of Fluid Mechanics **43**, 141 (2011).
[11] M. Heil and A. Hazel, "oomp-lib," `http://oomph-lib.maths.man.ac.uk/doc/html/index.html` (2006).
[12] M. Heil and A. L. Hazel, in *Fluid-structure interaction*, edited by M. Schäfer and H.-J. Bungartz (Springer, 2006) pp. 19–49.
[13] C. Tang, L.-D. Zhu, G. Akingba, and X.-Y. Lu, Journal of Biomechanics **48**, 1922 (2015).
[14] A. A. Shabana, *Theory of Vibration* (Springer-Verlag, 1991).
[15] N. Westerhof, J.-W. Lankhaar, and B. E. Westerhof, Med. Biol. Eng. Comput. **47**, 131 (2009).